

The Dielectric Response of Spherical Live Cells in Suspension: An Analytic Solution

Emil Prodan,* Camelia Prodan,[†] and John H. Miller, Jr.[‡]

*Physics Department, Yeshiva University, New York, New York; [†]Physics Department, New Jersey Institute of Technology, Newark, New Jersey; and [‡]Physics Department and Texas Center for Superconductivity, University of Houston, University of Houston, Houston, Texas

ABSTRACT We develop a theoretical framework to describe the dielectric response of live cells in suspensions when placed in low external electric fields. The treatment takes into account the presence of the cell's membrane and of the charge movement at the membrane's surfaces. For spherical cells suspended in aqueous solutions, we give an analytic solution for the dielectric function, which is shown to account for the α - and β -plateaus seen in many experimental data. The effect of different physical parameters on the dielectric curves is methodically analyzed.

INTRODUCTION

Dielectric spectroscopy has been successfully used in the past to characterize biological matter (1–8). These types of measurements probe the collective dielectric response of many live cells in suspensions or in tissues, but by using more or less elaborated models, useful information about the state of the individual cell can be also extracted (9). The main advantage of this technique is that it is noninvasive, thus the state of the individual cells can be monitored without disrupting their natural cycle. Sensing methods have been developed based on the difference in dielectric response between live and dead cells of *Escherichia coli* (10). Dielectric spectroscopy has been used to monitor the biomass concentration of *Bacillus thuringiensis* (11) and that of *Lactobacillus casei* (12) as well.

The dielectric response of live cells is fundamentally different from that of dead cells (10,13,14). From the dielectric point of view, the main difference between the two cases is the existence of the membrane potential in live cells. The effect of the membrane potential is an accumulation of mobile electric charge carriers at the membrane surfaces. When the live cells are placed in time-oscillating electric fields, these charges move on the surface of the membrane, giving rise to extremely high polarizations. Since the mobility of these surface charges is relatively small, this effect appears only at low frequencies, typically <10 kHz. In this range, the relative dielectric permittivity of live cell suspensions can be as high as 10^6 (15–17). This phenomenon is known as the α -relaxation effect. At higher frequencies, the α -effect disappears and a second interesting dielectric spectroscopic region appears, which is the β -relaxation. In this region, the dielectric function of a cell suspension is tremendously enhanced by the presence of cell's membrane alone.

In a previous article (18), we proposed a model for dielectric response of live cells in suspension, which could account for both α - and β -effects. Our focus in that work was to give a semianalytic expression for the dielectric function of suspended live cells of arbitrary shape. Because of the complexity of that problem, we adopted the powerful, but somewhat complicated, spectral method introduced by Bergman (19). In this article, we work out a fully analytic solution of the model proposed in Prodan and Prodan (18), for the case of spherically shaped cells. We hope that this analytic solution will provide a new useful tool for the scientific community working in this field.

The independent input parameters for our model are: the outer and inner radius of the cell's membrane, r_1 and r_2 ; the dielectric constant and conductivity of the medium (ϵ_0, σ_0), of the membrane (ϵ_1, σ_1) and of the inner cell region (ϵ_2, σ_2); the diffusion constants of surface charges accumulated at the outer and inner surfaces of the membrane, D_1 and D_2 ; and the membrane potential ΔV . Excepting ϵ_2 and D_2 , all these parameters have a very specific effect on the dielectric dispersion curves of live cells in suspension, leading us to conclude that a fitting of an experimental dispersion curve with the present model could provide extremely accurate values for all these parameters.

There is a tremendous amount of theoretical work on α -relaxation in colloids. Schwan et al. (20) is one of the earliest works that pointed out that the macroscopic dielectric function of colloidal suspensions is highly dependent, in the low frequency range, on the electrical phenomena taking place near the surface of colloidal particles. Schwarz (21) gave a first semiquantitative treatment of these effects. O'Brien and White (22) and DeLacey and White (23) developed the theoretical foundations for the second-layer polarization effect, and the work in the field culminated with Mangelsdorf and White (24), which gave what was thought to be a complete theory of electrophoretic mobility of charged colloidal particles. This theory computes the net drag force on charged colloidal particles in electrolytes and takes into

Submitted May 9, 2008, and accepted for publication July 16, 2008.

Address reprint requests to Emil Prodan, Tel.: 212-340-7831; E-mail: prodan@yu.edu.

Editor: Michael D. Stern.

© 2008 by the Biophysical Society
0006-3495/08/11/4174/09 \$2.00

doi: 10.1529/biophysj.108.137042

account the deformation of the screening cloud via linearized hydrodynamic equations. However, from early comparisons with the experiment (25), it was soon realized that, besides the electrophoretic effect, there is another effect, the α -relaxation, which dwarfs the first one in most of the cases. The early theory of electrophoretic mobility considered a rigid Stern layer. A complete theory will have to relax this assumption. Notable efforts in this direction are contained in a string of articles (26–29), which resulted in a fairly complicated theory of the polarization of the second layer. A discussion of latest developments in the field can be found in Delgado et al. (30), Shilov et al. (31), Carrique et al. (32), and Grozze and Shilov (33).

Our model complements these works and we could argue that it gives an effective picture of the α -polarization of the second layer. The dielectric behavior of live cells in suspension at low frequencies and low applied electric fields is predominantly determined by the α -relaxation. The theoretical model presented here specifically targets the α -relaxation process, thus allowing us to keep the complexity and number of input parameters to a minimum. Other theoretical works specifically addressing the dielectric response of live cells suspensions are contained in Vranceanu and Gheorghiu (34), Asami et al. (35), and Gheorghiu (36,37)—notably, a simple theory of α - and β -effects for spherically symmetric cells (37), and an early attempt for quantifying the β -effect for arbitrary geometry (34). Some later works (38,39) give alternative approaches to the β -effect.

MEMBRANE POTENTIAL AND α -RELAXATION

Live cells contain a large number of negatively charged molecules. The inside negative charge attracts positive charges from the outside, mainly potassium and sodium positive ions. The cells allow most of the potassium ions to enter inside, still maintaining an overall negative charge, while keeping most of the sodium ions outside. This gives rise to a sharp potential difference across the membrane, called the resting membrane potential. Its value can be anywhere in a range from 60 mV to a few tens over 100 mV. The electric field due to such potential differences is enormous. For example, 100 mV over a membrane of 10 nm gives an electric field of 10,000,000 V/m.

The charge distribution near the cell's membrane is schematically represented in Fig. 1 *a*. As discussed above, we have a positive ion distribution outside the membrane and a negative ion distribution inside the membrane. The exact radial profile of the charge distribution can be computed by solving the coupled equations describing the electrostatics and diffusion of ions near the membrane. However, the exact profile is not relevant for this study. What is important is that the distribution is confined to within a few nanometers from the surface of the membrane.

When an electric field is applied, the charge distribution is deformed as schematically shown in Fig. 1 *b*. This redistribution generates a large dipole moment, which is at the origin

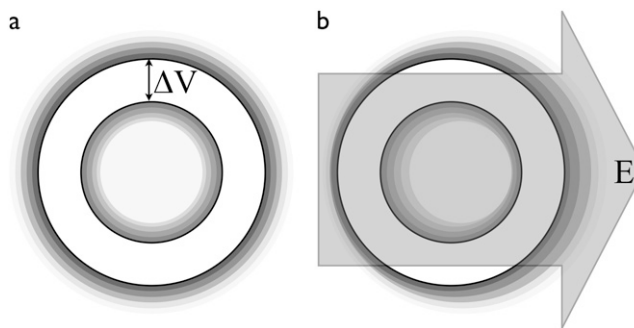


FIGURE 1 (a) Schematic representation of the ion charge accumulated around the membrane. (b) Schematic representation of the polarization of this charge when a driving electric field E is applied.

of the α -relaxation process (40–42). If the field is time-oscillating, the ions will try to follow the electric field and dynamically redistribute themselves. As we shall see, there is a sharp frequency above which the ions can no longer follow the electric field. Above this frequency, the polarizability of the cells drastically decreases and the α -effect disappears.

THE MODEL

Our goal is to propose and then solve analytically a model for the dielectric response of live cells in suspensions in the frequency range from 1 Hz to 100 MHz. In this range, the electromagnetic field cannot distinguish the very fine structure of the cell, but it rather sees an effective image of it. It is now generally accepted (40) that this effective image is well described by a composite dielectric body made of a dielectric shell representing the cell membrane (described here by (ϵ_1, σ_1)) and a homogeneous dielectric core (described here by (ϵ_2, σ_2)). Of course, the inside of a cell is very nonhomogeneous, but this is irrelevant since the field penetrates very little inside the cell at low frequencies. This simple picture of the cell is the starting point for most of the theoretical work in the field. The early work by Maxwell and Wagner (43), who studied the dielectric behavior of spherical dielectric particles in suspensions, is probably the most widely used theory to describe the dielectric response of cell suspensions (40).

On top of this static picture, our model assumes that the charge distributions near a cell's membrane can be described by effective superficial charge distributions ρ_1 and ρ_2 at the outer and inner faces of the membrane. These superficial distributions of charges are described by the following properties:

1. The values of $\rho_{1,2}$ are constrained to the faces $\Sigma_{1,2}$ of the membrane, so that they cannot leave these surfaces at any time.
2. The charges are free to move on the faces $\Sigma_{1,2}$ of the membrane. The movement, which is generated by gradients in the electric potential and in charge density, gives rise to singular electric currents

$$\vec{j}_{\text{sing}} = -\gamma_i \vec{\nabla}_{\Sigma_i} \Phi - D_i \vec{\nabla}_{\Sigma_i} \rho_i, \quad i = 1, 2, \quad (1)$$

where γ_i and D_i are the electrical conductivities and diffusion coefficients of the bound charges, respectively.

3. The external electric fields are considered small, so that the conductivities γ_i are given with good approximation by the charge distributions ρ_{0i} in the absence of any external fields,

$$\gamma_i = u_i \rho_{0i}, \quad i = 1, 2, \quad (2)$$

where u_i is the mobility of the bound charges on the two membrane's faces.

From now on, our study focuses on shelled particles with the properties described above, which are suspended in an electrolyte with dielectric constant ϵ_0 and conductivity σ_0 . We will use the symbol ϵ^* to denote the complex dielectric function defined as $\epsilon^* = \epsilon + \sigma/j\omega$. We are interested in the response of such suspensions when placed between the metallic plates of capacitors like in Fig. 2. In the linear regime of small electric fields, the complex system will behave like a dielectric material, whose dielectric function at given pulsation ω can be computed using Lorenz theory (44),

$$\epsilon^*(\omega) = \epsilon_0 \left(1 - \frac{p\alpha(\omega)}{1 - p\alpha(\omega)/3} \right), \quad (3)$$

where p is volume fraction occupied by the cells in solution and $\alpha(\omega)$ is the frequency-dependent polarizability:

$$\alpha = \frac{1}{E_0^2 V} \int_V dv \frac{\epsilon^* - \epsilon_0^*}{\epsilon_0^*} \vec{E}_0 \cdot \langle \vec{E} \rangle. \quad (4)$$

Here, \vec{E} is the total electric field when a single cell is placed in the external, homogeneous, time-oscillating electric field $E_0 e^{i\omega t}$ and V is the volume of one single cell. The $\langle \dots \rangle$ indicates the average over all possible orientations of the cell. For spherically shaped cells, this average has no effect.

MATHEMATICAL EQUATIONS OF THE MODEL

We write the equations of the model for arbitrarily shaped cells. If we focus on the polarizability $\alpha(\omega)$, we need to

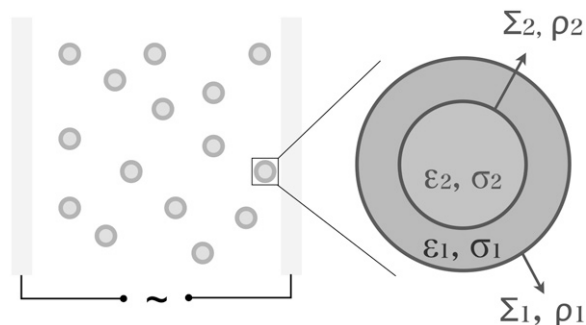


FIGURE 2 In dielectric spectroscopy experiments, a suspension of live cells is placed between the plates of a capacitor that is subjected to an AC signal, as shown in the left panel. The right panel shows our model for live cells.

consider the problem of a single cell placed in the external field $\vec{E}_0 e^{i\omega t}$.

The equations governing our model include the Laplace equation for the electric potential, $\vec{\nabla}^2 \Phi = 0$, the continuity equations for the constrained charges, $\vec{\nabla}_{\Sigma} \vec{j}_{\text{sing}} + \partial \rho_i / \partial t = 0$, together with the boundary conditions at the membrane surfaces. The usual boundary conditions at low frequency have to be modified due to the presence of ρ_i at the interfaces. Their new form can be derived from the conservation of charges. Indeed, let Σ be an interface, with a charge distribution ρ constrained on it (see Fig. 3) and assume that Σ separates two dielectric media \mathcal{D}_{\pm} . The electrical current flowing near the interface is composed by a volume 1, given by the usual expression $\vec{j}_{\text{vol}}^{\pm} = \sigma^{\pm} \vec{E}$, and a singular component, \vec{j}_{sing} flowing on the interface. Now, note that, whenever two joined media with different dielectric properties are placed in a time-oscillating electric field, free charges accumulate at the interface between them. This is because the amplitudes and the phases of the oscillations of the volumic charge carriers are different in the two sides of the interface. A typical example of such charge accumulation is the screening charge appearing at the interface between a metal and an insulator in the presence of an electric field. This means that on top of the constrained charge distribution ρ , additional free charges will accumulate on our dielectric interface, precisely because of the different conductivities σ^{\pm} . These additional charges behave differently from ρ , because they are free to leave the surface and they do not give rise to singular currents at the interface. Denoting by τ the net superficial charge distribution, the charge conservation for a domain Ω centered on the surface as shown in Fig. 3 gives

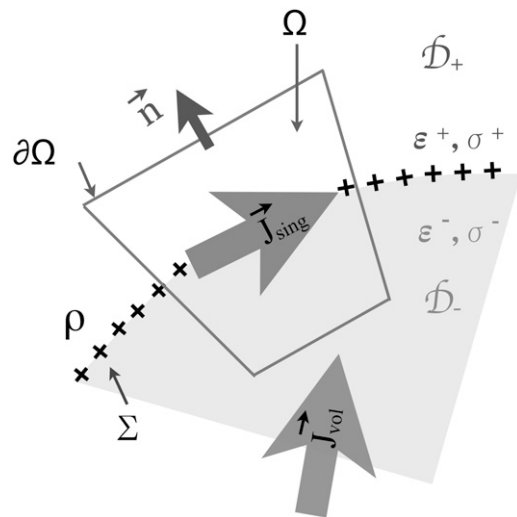


FIGURE 3 The interface Σ separates two electrolytes of different dielectric characteristics. A superficial charge distribution ρ is constrained at the interface Σ . Movement of these charges generates the singular current distribution \vec{j}_{sing} . The diagram also shows the usual volume current \vec{j}_{vol} in electrolytes and the volume Ω and its boundary $\partial\Omega$ used in the text.

$$-\frac{d}{dt} \int_{\Omega} \tau dv = \oint_{\partial\Omega} \vec{j}_{\text{vol}} d\vec{S} + \oint_{\Gamma} \vec{j}_{\text{sing}} d\vec{\Gamma}, \quad (5)$$

where Γ is the contour on the interface given by the intersection $\Gamma = \partial\Omega \cap \Sigma$. Using the Maxwell equation, $\tau = \vec{\nabla} \cdot \vec{D}$ and the divergence theorem, it follows

$$\oint_{\Gamma} \left(\sigma \vec{E} + \frac{\partial}{\partial t} \vec{D} \right) \cdot d\vec{S} = - \oint_{\Gamma} \vec{j}_{\text{sing}} d\vec{\Gamma}. \quad (6)$$

Noticing that the singular current is the only cause of the time variation of the superficial distribution,

$$-\frac{d}{dt} \int_{\Omega \cap \Sigma} \rho dS = \oint_{\Gamma} \vec{j}_{\text{sing}} d\vec{\Gamma}, \quad (7)$$

we arrive at the integral form of the boundary conditions,

$$\oint_{\Omega \cap \Sigma} \left(\sigma \vec{E} + \frac{\partial}{\partial t} \vec{D} \right) \cdot d\vec{S} = \frac{d}{dt} \int_{\Omega \cap \Sigma} \rho dS. \quad (8)$$

In the differential form, the boundary condition takes the form

$$\vec{n} \left(\sigma^+ \vec{E}^+ + \frac{\partial}{\partial t} \vec{D}^+ \right) - \vec{n} \left(\sigma^- \vec{E}^- + \frac{\partial}{\partial t} \vec{D}^- \right) = \frac{\partial \rho}{\partial t}, \quad (9)$$

where \vec{n} represents the normal at the interface (see Fig. 3). We can now write the complete set of equations for our model:

$$\begin{cases} \vec{\nabla}^2 \Phi = 0; & \vec{\nabla}_{\Sigma_i} \vec{j}_{\text{sing}} + \partial \rho_i / \partial t = 0. \\ \vec{n}(\sigma_{i-1} \vec{E}_i^+ + \frac{\partial}{\partial t} \vec{D}_i^+) - \vec{n}(\sigma_i \vec{E}_i^- + \frac{\partial}{\partial t} \vec{D}_i^-) = \frac{\partial \rho_i}{\partial t}. \\ \vec{E} \rightarrow \vec{E}_0 \exp(j\omega_0 t) \quad \text{as } |\vec{r}| \rightarrow \infty. \end{cases} \quad (10)$$

In the frequency domain:

$$\begin{cases} \vec{\nabla}^2 \Phi = 0; & \vec{\nabla}_{\Sigma_i} \vec{j}_{\text{sing}} + j\omega \rho_i = 0. \\ \epsilon_{i-1}^* \partial_n \Phi_i^+ - \epsilon_i^* \partial_n \Phi_i^- = -\rho_i. \\ \Phi \rightarrow 0 \quad \text{as } |\vec{r}| \rightarrow \infty. \end{cases} \quad (11)$$

THE EQUILIBRIUM CONFIGURATION

In the absence of external electric fields, we can set all time derivatives in Eq. 10 to zero and obtain

$$\begin{cases} \vec{\nabla}^2 \Phi = 0; & \vec{\nabla}_{\Sigma_i} \vec{j}_{\text{sing}} = 0. \\ \sigma_{i-1} \partial_n \Phi_i^+ - \sigma_i \partial_n \Phi_i^- = 0. \\ \Phi \rightarrow 0 \quad \text{as } |\vec{r}| \rightarrow \infty. \end{cases} \quad (12)$$

The above equations must be complemented by the condition

$$\int_{\Sigma_i} \rho_{0i} = \pm Q \quad (13)$$

for $i = 1, 2$, respectively. Here, Q is the total charge accumulated at the membrane surfaces and we introduced the additional index 0 for the surface constrained mobile charges ρ to specify that we are now discussing the distribution in the absence of any driving electric field.

This system of equations can be easily solved when the membrane's conductivity is set to zero, which we will do in the rest of the article. Indeed, the second row of Eq. 12 becomes

$$\sigma_0 \partial_n \Phi_1^+ = 0 \quad \text{and} \quad \sigma_2 \partial_n \Phi_2^- = 0, \quad (14)$$

which actually represent trivial Neumann boundary conditions for the Laplace equation on the outside and inside regions of the cell. Consequently, at equilibrium, the potential is constant inside these regions. Now the equation $\vec{\nabla}_{\Sigma_i} \vec{j}_{\text{sing}} = 0$ becomes

$$\vec{\nabla}_{\Sigma_i} \left[\gamma_i \vec{E}_{\text{tangent}} - D_i \vec{\nabla} \rho_{0i} \right] = -D_i \vec{\nabla}^2 \rho_{0i} = 0 \quad (15)$$

with a unique solution $\rho_{0i} = \text{constant}$,

$$\rho_{0i} = \pm \frac{Q}{\text{Area}_{\Sigma_i}}, \quad i = 1, 2. \quad (16)$$

Notice that, unlike ρ_{0i} , the total superficial charge τ_i at the interfaces is not uniformly distributed. Finally, the total charge $\pm Q = \int_{\Sigma_i} \tau_i dS$ is related to the resting membrane potential by

$$Q = C \Delta V, \quad (17)$$

where C is the membrane capacitance.

Since $\int_{\Sigma_i} \tau_i dS = \int_{\Sigma_{0i}} \rho_i dS$, we can state now the main conclusion of the section: independent of the shape of the cell, the conductivity of the superficial charges ρ_i , given in Eq. 2, is constant. This constant is controlled by the membrane potential

$$\gamma_i = u_i \frac{C \Delta V}{\text{Area}_{\Sigma_i}}. \quad (18)$$

We point out that the diffusion constant D and the conductivity γ at the membrane surface are related through Einstein relation ($k_B =$ Boltzmann constant),

$$qD = uk_B T, \quad (19)$$

which, together with Eqs. 2 and 18, gives

$$\Delta V = \frac{k_B T}{q} \frac{\gamma_i \text{Area}_{\Sigma_i}}{D_i C}. \quad (20)$$

Using the formula for thin, planar capacitors, $C = \epsilon S/d$, at room temperature $T = 24^\circ\text{C}$, we have

$$\Delta V = 3.00 \frac{\gamma_i}{D_i \epsilon_1 / \epsilon_{\text{vac}}}, \quad (21)$$

where $d = r_1 - r_2$ is measured in nanometers. The last relation also shows that the ratios γ_1/D_1 and γ_2/D_2 must be the same.

We remind that the model cannot predict ΔV ; instead, as mentioned in the Introduction, ΔV is one of our input parameters. ΔV can be obtained either through direct (like patch-clamping) or indirect (like using the Goldman-Hodgkin-Katz theory on the ionic concentrations) experiments. We should point out that the formula in Eq. 21 for the membrane potential only shows the relation between ΔV and the conductivity of the mobile charges. The mobility of charges also appears in this relation, but we chose to work with the dif-

fusion constant D instead of the mobility because people are more familiar with the first one. Also, it is γ and D that enter directly in the equations of the model.

THE ANALYTIC SOLUTION FOR SPHERICAL CELLS

We use the single-layer expression for the electrostatic potential

$$\Phi(\vec{r}) = -zE_0 + \frac{1}{4\pi} \int_{\Sigma_1} \frac{\mu_1(\vec{r}')}{|\vec{r} - \vec{r}'|} dS_{r'} + \frac{1}{4\pi} \int_{\Sigma_2} \frac{\mu_2(\vec{r}')}{|\vec{r} - \vec{r}'|} dS_{r'}, \quad (22)$$

where we took the z axis along \vec{E}_0 . Our goal is to solve for the charge distributions μ_1 and μ_2 . They are determined by the following equations:

$$\begin{cases} \gamma_i \vec{\nabla}_{\Sigma_i}^2 \Phi + D_i \vec{\nabla}_{\Sigma_i}^2 \rho_i = j\omega \rho_i \\ \epsilon_{i-1}^* \partial_n \Phi_i^+ - \epsilon_i^* \partial_n \Phi_i^- = \rho_i \end{cases} \quad (23)$$

On the sphere, we have the expression

$$\vec{\nabla}_{\Sigma_i}^2 = \frac{1}{R_i^2 \sin^2 \theta} \frac{\partial}{\partial \theta} \left(\sin \theta \frac{\partial}{\partial \theta} \right) + \frac{1}{R_i^2 \sin^2 \theta} \frac{\partial^2}{\partial \phi^2}, \quad (24)$$

where θ and ϕ are the usual spherical coordinates.

The distributions μ_i can be expanded in the spherical harmonic functions $Y_{lm}(\theta, \phi)$. Since the external field is homogeneous, only the $l = 1$ and $m = 0$ terms will be actually present:

$$\mu_1(\vec{r}) = p_1 Y_{10}(\theta), \quad \mu_2(\vec{r}) = p_2 Y_{10}(\theta). \quad (25)$$

Using

$$\frac{1}{|\vec{r} - \vec{r}'|} = 4\pi \sum_{lm} v_l(r, r') Y_{lm}(\theta, \phi) Y_{lm}^*(\theta', \phi') \quad (26)$$

with

$$v_l(r, r') = \frac{1}{2l+1} \frac{r_{<}^l}{r_{>}^{l+1}} \quad (27)$$

and the ortho-normalization of the spherical harmonics, we obtain

$$\begin{aligned} \Phi(\vec{r}) &= [-r\vec{E}_0 + p_1 v_1(r, r_1) + p_2 v_1(r, r_2)] Y_{10}(\theta) \\ &\left(\vec{E}_0 = \sqrt{\frac{4\pi}{3}} E_0 \right). \end{aligned} \quad (28)$$

Using similar arguments for the ρ_i distributions, we write

$$\rho_1(\vec{r}) = q_1 Y_{10}(\theta), \quad \rho_2(\vec{r}) = q_2 Y_{10}(\theta). \quad (29)$$

Given that Y_{10} is an eigenfunction of the Laplace operator of eigenvalue $-2/R^2$, we obtain the following algebraic equations for p_1, p_2, q_1 , and q_2 :

$$\begin{aligned} \left(-r_1 \vec{E}_0 + \frac{p_1}{3r_1} + \frac{r_2 p_2}{3r_1^2} \right) \frac{2\gamma_1}{r_1^2} + D_1 \frac{2q_1}{r_1^2} &= -j\omega q_1 \\ \left(-r_2 \vec{E}_0 + \frac{r_2 p_1}{3r_1^2} + \frac{p_2}{3r_2} \right) \frac{2\gamma_2}{r_2^2} + D_2 \frac{2q_2}{r_2^2} &= -j\omega q_2 \\ (\epsilon_1^* - \epsilon_0^*) \vec{E}_0 - \frac{\epsilon_1^* + 2\epsilon_0^*}{3r_1^2} p_1 + \frac{2(\epsilon_1^* - \epsilon_0^*) r_2}{3r_1^3} p_2 &= -q_1 \\ (\epsilon_2^* - \epsilon_1^*) \vec{E}_0 + \frac{\epsilon_1^* - \epsilon_2^*}{3r_1^2} p_1 - \frac{\epsilon_2^* + 2\epsilon_1^*}{3r_2^2} p_2 &= -q_2. \end{aligned} \quad (30)$$

The solution is

$$\begin{aligned} p_1 &= \frac{C - B}{AC - B} 3r_1^2 \vec{E}_0, \\ p_2 &= \frac{A - 1}{AC - B} 3r_1^2 \vec{E}_0, \end{aligned} \quad (31)$$

where

$$\begin{aligned} A &= \frac{2r_1 \gamma_1 + (2D_1 + j\omega r_1^2)(\epsilon_1^* + 2\epsilon_0^*)}{2r_1 \gamma_1 + (2D_1 + j\omega r_1^2)(\epsilon_1^* - \epsilon_0^*)} \\ B &= \frac{2r_2 \gamma_1 - 2(2D_1 + j\omega r_1^2)(\epsilon_1^* - \epsilon_0^*) r_2 / r_1}{2r_1 \gamma_1 + (2D_1 + j\omega r_1^2)(\epsilon_1^* - \epsilon_0^*)} \\ C &= \frac{r_1^2 2r_2 \gamma_2 + (2D_2 + j\omega r_2^2)(\epsilon_2^* + 2\epsilon_1^*)}{r_2^2 2r_2 \gamma_2 + (2D_2 + j\omega r_2^2)(\epsilon_2^* - \epsilon_1^*)}. \end{aligned} \quad (32)$$

The polarizability of the cells can be computed directly from Eq. 4, using $\vec{E} = -\vec{\nabla}\Phi$ and the explicit expression of the electrostatic potential given in Eq. 28:

$$\begin{aligned} \alpha &= \frac{\epsilon_1^* - \epsilon_0^*}{\epsilon_0^*} \left[1 - \frac{p_1}{3r_1^2} \right] \left[1 - \left(\frac{r_2}{r_1} \right)^3 \right] \\ &+ \frac{\epsilon_2^* - \epsilon_0^*}{\epsilon_0^*} \left[1 - \frac{p_1}{3r_1^2} - \frac{p_2}{3r_2^2} \right] \left(\frac{r_2}{r_1} \right)^3. \end{aligned} \quad (33)$$

Equation 3 together with Eqs. 31–33 represent our analytic solution.

ANALYSIS

In Fig. 4, we report a dielectric dispersion curve of the dielectric permittivity generated with the present model. The geometrical and dielectric input parameters were chosen similar to those used in Stoneman et al. (9) to fit experimental dielectric curves of live yeast cells in a buffer solution (see Fig. 3 of this reference). We chose the volume concentration to be $p = 0.1$. The β -dispersion in our theoretical graph matches very closely the experimental findings. Unfortunately, Stoneman et al. (9) was not able to resolve the α -dispersion. In our theoretical graph, one can clearly distinguish the α -dispersions at $\sim 10^3$ Hz. The shape of the entire dispersion curve for the dielectric function resembles quite well the experimentally measured curves of Bordi et al. (13) for erythrocytes or of Raicu et al. (17) for mammalian cells. Both references report data in the α -relaxation fre-

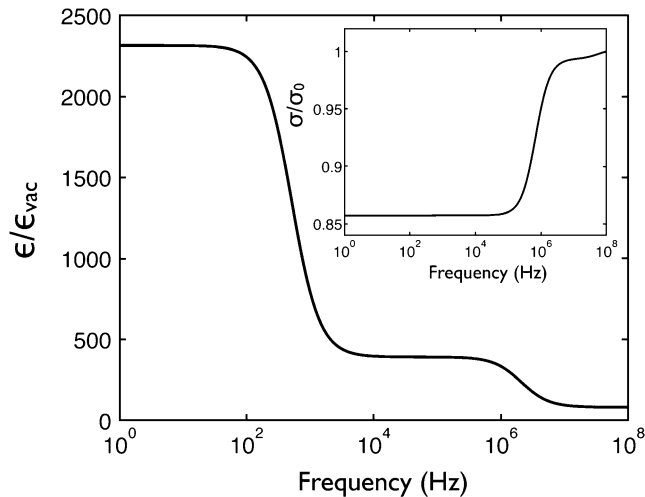


FIGURE 4 Dispersion curves of $\varepsilon(\omega)$ for $r_1 = 2.5 \mu\text{m}$; $r_2 = 2.4975 \mu\text{m}$ (membrane thickness of 2.5 nm); $\sigma_0 = 0.28$; $\sigma_1 = 0$; $\sigma_2 = 0.275$; $\varepsilon_0 = 78$; $\varepsilon_1 = 1.6$; $\varepsilon_2 = 125$; $D_1 = 10^{-8}$; $D_2 = 10^{-8}$; $\gamma_1/D_1 = 0.1$; and $\gamma_2/D_2 = 0.1$. The inset shows the dispersion of the conductivity σ . The numbers represent SI units.

quency region. In these experimental works, the plateau between α - and β -dispersions was found to be at a dielectric permittivity of 10^3 for erythrocytes (13), and at much higher values (between 10^4 and 10^5) for liver cells of rats (17). These are quite high values when compared with the value of ~ 500 for yeast cells. As we will show below, this plateau moves up quite sharply as the radius of the cell is increased and, since the mammalian cells are much larger than the yeast cells, this could explain the difference. The experimental works reported a value of $\sim 10^6$ for the plateau before the α -relaxation. In Fig. 4, we also show the dispersion curve of the conductivity, which indicate an almost flat behavior of σ with the frequency.

In the following, we analyze the effect of variations in the different parameters of the model. We start by pointing out that D_2 , γ_2 , and ε_2 have very little influence on the dielectric properties of the suspension. This confirms the assumption made in Prodan and Prodan (18) that the charge distribution ρ_2 on the inner surface of the membrane plays little role in the α -relaxation. This is understandable because the electric field penetrates little inside the cell.

The conductivities of the outer and inner regions of the cell, σ_0 and σ_2 , on the other hand, have very specific and similar effects in the β -region. From Figs. 5 and 6, one can see that σ_0 and σ_2 control the frequency of the β -dispersion: the larger the σ_0 or σ_2 value, the larger the frequency of the β -dispersion. For example, by varying σ_2 from 0.001 to 0.1, which is an appropriate range for σ inside the cell, we observe a shift of the β -dispersion from $\sim 10^3$ to 10^5 . We want to mention that, since the potassium ions are taken in by the cells, σ_2 can be modified by changing the potassium concentration of the solution. The value σ_0 can be modified by, for example, modifying the sodium concentration of the solution.

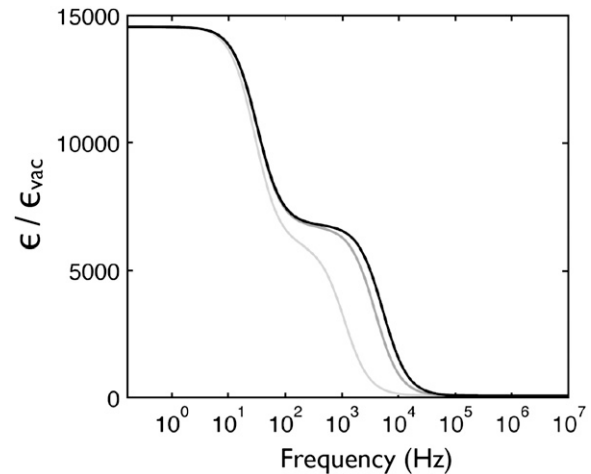


FIGURE 5 Dispersion curve of $\varepsilon(\omega)$ for $r_1 = 10 \mu\text{m}$; $r_2 = 9.997 \mu\text{m}$; $\sigma_0 = 0.001$ (light shaded); 0.01 (dark shaded); 0.1 (solid); $\sigma_1 = 0$; $\sigma_2 = 0.01$; $\varepsilon_0 = 78$; $\varepsilon_1 = 10$; $\varepsilon_2 = 80$; $D_1 = 10^{-8}$; $D_2 = 10^{-8}$; $\gamma_1/D_1 = 0.1$; and $\gamma_2/D_2 = 0.1$. The numbers represent SI units.

The thickness of the membrane also has a very specific effect on the plateau between the α - and β -dispersions. From Fig. 7, one can see that the membrane thickness controls the height of this plateau: the smaller the thickness the higher the plateau. Note that the height of the plateau before the α -dispersion also changes in Fig. 7. However, these changes are exactly equal to the changes in the plateau before the β -dispersion, suggesting that the membrane thickness does not affect the α -response of the cells.

We now focus on Fig. 8, where we fixed $d = 3 \text{ nm}$ and let $\gamma_1/D_1 = \gamma_2/D_2$ take the values 0.01, 0.05, and 0.1. This implies the following values for the membrane potential ΔV : 9, 45, and 90 mV, respectively. We point out that the membrane potential ΔV of live cells in suspension can be modified by

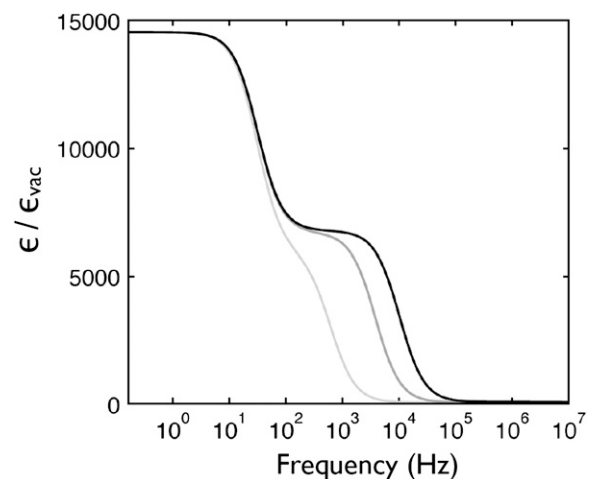


FIGURE 6 Dispersion curves of $\varepsilon(\omega)$ for $r_1 = 10 \mu\text{m}$; $r_2 = 9.997 \mu\text{m}$; $\sigma_0 = 0.01$; $\sigma_1 = 0$; $\sigma_2 = 0.001$ (light shaded); 0.01 (dark shaded); 0.1 (solid); $\varepsilon_0 = 78$; $\varepsilon_1 = 10$; $\varepsilon_2 = 80$; $D_1 = 10^{-8}$; $D_2 = 10^{-8}$; $\gamma_1/D_1 = 0.1$; and $\gamma_2/D_2 = 0.1$. The numbers represent SI units.

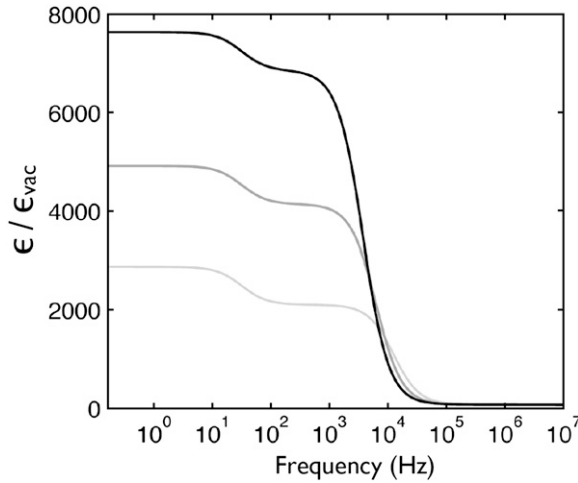


FIGURE 7 Dispersion curves of $\varepsilon(\omega)$ for $r_1 = 10 \mu\text{m}$; $r_2 = 9.99 \mu\text{m}$ (light shaded); $9.995 \mu\text{m}$ (dark shaded); $9.997 \mu\text{m}$ (solid); $\sigma_0 = 0.01$; $\sigma_1 = 0$; $\sigma_2 = 0.01$; $\varepsilon_0 = 78$; $\varepsilon_1 = 10$; $\varepsilon_2 = 80$; $D_1 = 10^{-8}$; $D_2 = 10^{-8}$; $\gamma_1/D_1 = 0.01$; and $\gamma_2/D_2 = 0.01$. The numbers represent SI units.

changing the potassium ion concentration (45) or by actively blocking or activating the ion channels (3,2). As one can see in Fig. 8, changes in the membrane potential have very specific and dramatic effects in the α -region: the larger the membrane potential, the stronger the α -dispersion. For the variations in the membrane potential mentioned above, the model predicts variations of the plateau before the α -dispersion of $\sim 8 \times 10^3$. We want to point out that such variations were seen experimentally in measurements on skeletal muscle cells (46,47). The experimental results, reported in these two works, show clear and dramatic change in the plateau before the α -dispersion when the muscle cells were depolarized during oxygen deprivation (ischemia).

At last, we discuss the effect of the mobility of surface charges, which is shown in Fig. 9. Changes in the mobility of

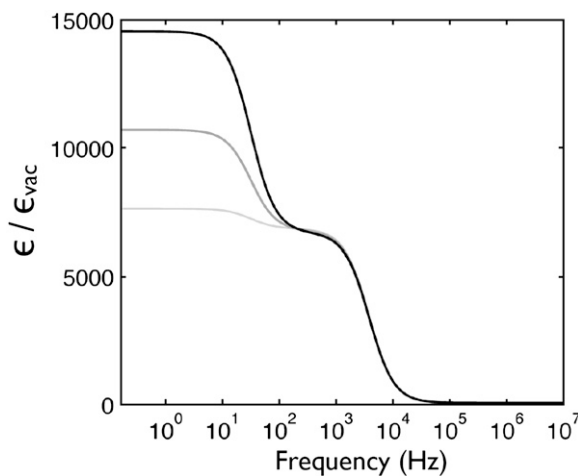


FIGURE 8 Dispersion curves of $\varepsilon(\omega)$ for $r_1 = 10 \mu\text{m}$; $r_2 = 9.997 \mu\text{m}$; $\sigma_0 = 0.01$; $\sigma_1 = 0$; $\sigma_2 = 0.01$; $\varepsilon_0 = 78$; $\varepsilon_1 = 10$; $\varepsilon_2 = 80$; $D_1 = 10^{-8}$; $D_2 = 10^{-8}$; $\gamma_1/D_1 = 0.1$; $\gamma_2/D_2 = 0.1$ (light shaded); 0.05 (dark shaded); and 0.1 (solid). The numbers represent SI units.

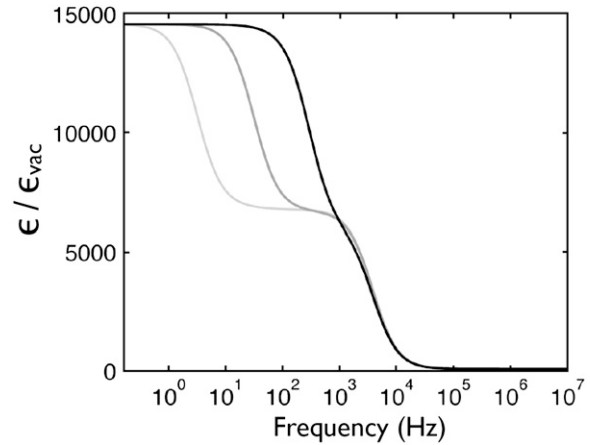


FIGURE 9 Dispersion curves of $\varepsilon(\omega)$ for $r_1 = 10 \mu\text{m}$; $r_2 = 9.997 \mu\text{m}$; $\sigma_0 = 0.01$; $\sigma_1 = 0$; $\sigma_2 = 0.01$; $\varepsilon_0 = 78$; $\varepsilon_1 = 10$; $\varepsilon_2 = 80$; $D_1 = 10^{-9}$ (light shaded); 10^{-8} (dark shaded); 10^{-7} (solid); $D_2 = 10^{-8}$; $\gamma_1/D_1 = 0.1$; and $\gamma_2/D_2 = 0.1$. The numbers represent SI units.

the surface charges also have a very specific and dramatic effect in the α -region, namely, the α -dispersion moves to right as the mobility is increased.

CONCLUSIONS

The first goal of our article was to propose a model that can account in a unified way for the dielectric response of live cells in suspensions in both α - and β -regions. The second goal of the article was to give an analytic solution to the model for the simple spherical geometry, a solution that could be useful for many people working in the field.

Based on this model, we have analyzed the effect of different physical parameters on the dielectric dispersion curves of live cells in suspension. We found that the conductivities of the medium and of the intracellular fluid control the length of the β -plateau, while the membrane thickness controls the height of the β -plateau. In the α -region, we found that the membrane potential controls the height of the α -plateau while the mobility of the surface charges accumulated at the cell's membrane controls the length of the α -plateau. All the parameters of the model have distinct influences on the dispersion curves, a fact that lead us to conclude that all the parameters can be accurately obtained by fitting experimental data with our model. Thus, the combination of experimental dielectroscopy data and our model could lead to a methodology for live cell monitoring.

Our results show that, for a given cell concentration and geometry, the low-frequency α -dielectric response correlates with the magnitude of the cellular membrane potential. This is potentially very important because it enables dielectric spectroscopy to become perhaps the only method for monitoring membrane potential that is both label free and noninvasive. For example, the use of voltage-sensitive dyes is problematic if one wishes to monitor, simultaneously, other

physiological processes such as ATP/ADP ratio, which require different fluorescent assays. As a result, if one wishes to study the effects of membrane potential on other parameters with conventional methods, it is often necessary to use fluorescent assays on two separate cell populations and then to correlate the results with the hope that the two populations are identical. A major advantage of dielectric spectroscopy, if further developed, is that one could use dielectric response to monitor membrane potential while using a fluorescent assay to monitor, simultaneously, another parameter on the same cell population. Moreover, dielectric response appears well suited to flow-cytometry and can be readily scaled into multielectrode (plate reader) systems and large-scale microfluidic devices. Therefore, we believe the method has potential for numerous applications, including fundamental research in cell biology and biochemistry, pharmaceutical development, and diagnostic methods in medicine.

This work was supported, in part, by the NJIT-ADVANCE grant awarded by the National Science Foundation (grant No. 0547427), and the Texas Center for Superconductivity and the Robert A. Welch Foundation (grant No. E-1221). J.H.M. also acknowledges support by grant No. R21 CA133153 from the National Heart, Lung, and Blood Institute and the National Cancer Institute, National Institutes of Health, and from the National Science Foundation. E.P. acknowledges financial support from the Yeshiva University.

REFERENCES

- Asami, K., and T. Yamaguchi. 1992. Dielectric spectroscopy of plant protoplasts. *Biophys. J.* 63:1493–1499.
- Păunescu, T. G., and S. I. Helman. 2001. cAMP activation of apical membrane Cl^- channels: theoretical considerations for impedance analysis. *Biophys. J.* 81:838–851.
- Păunescu, T. G., and S. I. Helman. 2001. PGE² activation of apical membrane Cl^- channels in A6 epithelia: impedance analysis. *Biophys. J.* 81:852–866.
- Lynch, B. P., A. M. Hilton, and G. J. Simpson. 2006. Nanoscale dielectrophoretic spectroscopy of individual immobilized mammalian blood cells. *Biophys. J.* 91:2678–2686.
- Sanabria, H., J. H. Miller, A. Mershin, R. F. Luduena, A. A. Kolomenski, H. A. Schuessler, and D. V. Nanopoulos. 2006. Impedance spectroscopy of α - β tubulin heterodimer suspensions. *Biophys. J.* 90:4644–4650.
- Awayda, M. S., W. V. Driessche, and S. I. Helman. 1999. Frequency-dependent capacitance of the apical membrane of frog skin: dielectric relaxation processes. *Biophys. J.* 76:219–232.
- Kyle, A. H., C. T. Chan, and A. I. Minchinton. 1999. Characterization of three-dimensional tissue cultures using electrical impedance spectroscopy. *Biophys. J.* 76:2640–2648.
- Prodan, C., J. Claycomb, E. Prodan, and J. H. Miller. 2000. High-TC squid-based impedance spectroscopy of living cell suspensions. *Phys. C Superconduct. Appl. IV.* 341–348:2693–2693.
- Stoneman, M., A. Chaturvedi, D. Jansma, M. Kosempa, C. Zeng, and V. Raicu. 2007. Protein influence on the plasma membrane dielectric properties: in vivo study utilizing dielectric spectroscopy and fluorescence microscopy. *Bioelectrochemistry.* 70:542–550.
- Jonsson, M., K. Welch, S. Hamp, and M. Stromme. 2006. Bacteria counting with impedance spectroscopy in a micro probe station. *J. Phys. Chem. B.* 110:10165–10169.
- Sarrafzadeh, M. H., L. Belloy, G. Esteban, J. M. Navarro, and C. Ghommidh. 2005. Dielectric monitoring of growth and sporulation of *Bacillus thuringiensis*. *Biotechnol. Lett.* 27:511–517.
- Arnoux, A. S., L. Belloy, G. Esteban, P. Teissier, and C. Ghommidh. 2005. Lactic acid bacteria biomass monitoring in highly conductive media by permittivity measurements. *Biotechnol. Lett.* 27:1511–1557.
- Bordi, F., C. Cametti, and T. Gili. 2001. Reduction of the contribution of electrode polarization effects in the radiowave dielectric measurements of highly conductive biological cell suspensions. *Bioelectrochemistry.* 54:53–61.
- Schwan, H. 1957. *Advances in Biological and Medical Physics*, Vol. 5. Academic Press, New York.
- Stoy, R., K. Foster, and H. Schwan. 1982. Dielectric properties of mammalian tissues from 0.1 to 100 MHz: a summary of recent data. *Phys. Med. Biol.* 27:501–513.
- Prodan, C., F. Mayo, J. Claycomb, J. H. Miller, and M. J. Benedik. 2004. Low-frequency, low-field dielectric spectroscopy of living cell suspensions. *J. Appl. Phys.* 95:3754–3756.
- Raicu, V., T. Saibara, and A. Irimajiri. 1998. Dielectric properties of rat liver in vivo: a noninvasive approach using an open-ended coaxial probe at audio/radio frequencies. *Bioelectrochem. Bioenerg.* 47:325–332.
- Prodan, C., and E. Prodan. 1999. The dielectric behavior of living cell suspensions. *J. Phys. D Appl. Phys.* 32:335–343.
- Bergman, D. 1978. The dielectric constant of a composite material—a problem in classical physics. *Phys. Rep.* 43:377–407.
- Schwan, H., G. Schwarz, J. Maczuk, and H. Pauly. 1962. On the low frequency dielectric dispersion of colloidal particles in electrolyte solution. *J. Phys. Chem.* 66:2626–2635.
- Schwarz, G. 1962. A theory of the low frequency dielectric dispersion of colloidal particles in electrolyte solution. *J. Phys. Chem.* 66:2626–2642.
- O'Brien, R., and L. White. 1978. Electrophoretic mobility of a spherical colloidal particle. *J. Chem. Soc., Faraday Trans. 2.* 74:1607–1626.
- DeLacey, E., and L. White. 1982. The polarization impedance of an ideally polarizable plane electrode. *J. Chem. Soc., Faraday Trans. 2.* 78:457–479.
- Mangelsdorf, C., and L. White. 1990. Effects of Stern-layer conductance on electrokinetic transport properties of colloidal particles. *J. Chem. Soc., Faraday Trans.* 86:2859–2870.
- Zukoskil, C., and D. Saville. 1986. The interpretation of electrokinetic measurements using a dynamic model of the Stern layer. *J. Colloid Interface Sci.* 114:32–44.
- Mangelsdorf, C., and L. White. 1990. Electrophoretic mobility of a spherical colloidal particle in an oscillating electric field. *J. Chem. Soc., Faraday Trans.* 88:3567.
- Mangelsdorf, C., and L. White. 1992. Dielectric response of a dilute suspension of spherical colloidal particles to an oscillating electric field. *J. Chem. Soc., Faraday Trans.* 88:3567–3581.
- Mangelsdorf, C., and L. White. 1998. The dynamic double layer. *J. Chem. Soc., Faraday Trans.* 94:2441–2452.
- Grosse, C., M. Tirado, W. Pieper, and R. Pottel. 1998. Broad frequency range study of the dielectric properties of suspensions of colloidal polystyrene. *J. Colloid Interface Sci.* 205:26–41.
- Delgado, A., F. Gonzalez-Caballero, F. Arroyo, F. Carrique, S. Dukhin, and I. Ruzilov. 1998. Low frequency dielectric dispersion in ethylcellulose latex. *Colloid Surf. A.* 131:95–107.
- Shilov, V., A. Delgado, F. Gonzalez-Caballero, J. Horno, J. Lopez-Garcia, and C. Grosse. 2000. Polarization of the electrical double layer. Time evolution after application of an electric field. *J. Colloid Interface Sci.* 232:141–148.
- Carrique, F., F. Arroyo, V. Shilov, J. Cuquejo, M. Jimenez, and A. Delgado. 2007. Effects of stagnant-layer conductivity on the electrical permittivity of concentrated colloidal suspensions. *J. Chem. Phys.* 126:104903–1–9.
- Grozze, C., and V. Shilov. 2007. Dependence of the dielectric properties of suspensions on the volume fraction of suspended particles. *J. Colloid Interface Sci.* 309:283–288.
- Vranceanu, D., and E. Gheorghiu. 1996. Shape effects on the dielectric behavior of arbitrarily shaped particles with particular reference to biological cells. *Bioelectrochemistry.* 40:167–170.

35. Asami, K., T. Yonezawa, H. Wakamatsu, and N. Koyanagi. 1996. Dielectric spectroscopy of biological cells. *Bioelectrochem. Bioenerg.* 40:141–145.
36. Gheorghiu, E. 1993. The resting potential in relation to the equivalent complex permittivity of a spherical cell suspension. *Phys. Med. Biol.* 38:979–982.
37. Gheorghiu, E. 1994. The dielectric behavior of suspensions of spherical cells: a unitary approach. *J. Phys. A. Math General.* 27:3883–3893.
38. Lei, J., J. Wan, K. Yu, and H. Sun. 2001. First-principle approach to dielectric behavior of nonspherical cell. *Phys. Rev. E Stat. Nonlin. Soft Matter Phys.* 64:012903-1–4.
39. Sancho, M., G. Martinez, and C. Martin. 2003. Accurate dielectric modeling of shelled particles and cells. *J. Electrostat.* 57:143–156.
40. Foster, K., and H. Schwan. 1989. Dielectric properties of tissues and biological materials: a critical review. *Crit. Rev. Biomed. Eng.* 17:25–104.
41. Watanabe, M., T. Suzaki, and A. Irimajiri. 1991. Dielectric behavior of frog lenses in the 100 Hz to 500 MHz range. *Biophys. J.* 59:139–149.
42. Marx, G., and C. Davey. 1999. The dielectric properties of biological cells at radiofrequencies: applications in biotechnology. *Enzyme Microb. Technol.* 25:161–171.
43. Wagner, K. 1914. Explanation of the dielectric after-effect processes on the basis of Maxwell ideas. *Archiv fur Electrotechnik.* 2:371–387.
44. Stratton, J. A. 1941. *Electromagnetic Theory*. McGraw-Hill, New York.
45. Suzuki, H., Z. Wang, M. Yamakoshi, and T. Nozawa. 2003. Probing the transmembrane potential of bacterial cells by voltage-sensitive dyes. *Anal. Sci.* 19:1239–1242.
46. Schaefer, M., H. J. Kirlum, C. Schlegel, and M. M. Gebhard. 1999. Dielectric properties of skeletal muscle during ischemia in the frequency range from 50 Hz to 200 MHz. *Ann. N. Y. Acad. Sci.* 873: 59–64.
47. Schaefer, M., W. Gross, J. Ackemann, and M. M. Gebhard. 2002. The complex dielectric spectrum of heart tissue during ischemia. *Bioelectrochemistry.* 58:171–180.